Osteogenic and Antimicrobial Nanoparticulate Calcium Phosphate and Poly-(D, L-Lactide-co-Glycolide) Powders for the Treatment of Osteomyelitis

Vuk Uskoković[1], **Charles Hoover**[2], **Marija Vukomanović**[3,4], **Dragan P. Uskoković**[3], and **Tejal A. Desai**[1]

[1]Therapeutic Micro and Nanotechnology Laboratory, Department of Bioengineering and Therapeutic Sciences, University of California, San Francisco, CA, USA

[2]Department of Cell and Tissue Biology, University of California, San Francisco, CA, USA

[3]Institute of Technical Sciences, Serbian Academy of Sciences and Arts, Belgrade, Serbia

[4]Advanced Materials Department, Jožef Stefan Institute, Ljubljana, Slovenia

Abstract

Development of a material for simultaneous sustained and localized delivery of antibiotics and induction of spontaneous regeneration of hard tissues affected by osteomyelitis stands for an important clinical need. In this work, a comparative analysis of the bacterial and osteoblastic cell response to two different nanoparticulate carriers of clindamycin, an antibiotic commonly prescribed in the treatment of bone infection, one composed of calcium phosphate and the other comprising poly-(D,L-lactide-co-glycolide)-coated calcium phosphate, was carried out. Three different non-cytotoxic phases of calcium phosphate, exhibiting dissolution and drug release profiles in the range of one week to two months to one year, respectively, were included in the analysis: monetite, amorphous calcium phosphate and hydroxyapatite. Spherical morphologies and narrow size distribution of both types of nanopowders were confirmed in transmission and scanning electron microscopic analyses. The antibiotic-containing powders exhibited sustained drug release contingent upon the degradation rate of the carrier. Assessment of the antibacterial performance of the antibiotic-encapsulated powders against *Staphylococcus aureus*, the most common pathogen isolated from infected bone, yielded satisfactory results both in broths and on blood agar plates for all the analyzed powders. In contrast, no cytotoxic behavior was detected upon the incubation of the antibiotic powders with the osteoblastic MC3T3-E1 cell line for up to three weeks. The cells were shown to engage in a close contact with the antibiotic-containing particles, irrespective of their internal or surface phase composition, polymeric or mineral. At the same time, both types of particles upregulated the expression of osteogenic markers osteocalcin, osteopontin, Runx2 and protocollagen type I, suggesting their ability to promote osteogenesis and enhance remineralization of the infected site in addition to eliminating the bacterial source of infection.

1. Introduction

Due to the increasing population of elderly, the incidence of osteomyelitis, inflammation of bone caused by pyogenic bacteria mainly found in healthy oral flora, is expected to rise in the future, alongside other bone diseases [1]. Osteomyelitis is particularly prevalent in the facial skeleton due to its accessibility to a variety of external pathogens and commensal microorganisms [2]. It also presents a major complication ensuing orthopedic and maxillofacial surgeries [3] as well as routine dental extractions [4]. Timely treatment of osteomyelitis is required to prevent it from spreading throughout the body and causing systemic osteonecrosis or facial disfigurement, as in the case of maxillofacial ostemyelitis. The typical treatment regimen for bone infection consists of: (a) intravenous administration of antibiotics lasting for 2 – 6 weeks, frequently followed by a 6-month course of oral antibiotics in the case of chronic infection; and (b) surgical removal of bone that has undergone necrosis due to restriction of blood flow by the formed abscesses [5, 6]. However, in the advanced stages of infection, when bone necrosis has become significant, the blood supply to the infected area is inadequate and the lesion is largely inaccessible to antimicrobial agents transported by the blood stream. Correspondingly, the two major downsides of the conventional therapeutic approach include: (a) nonlocal distribution of therapeutic agents around the site of infection, with low concentration prone to induce resistance of the pathogen to the antibiotic therapy; and (b) irretrievable bone loss that often demands insertion of implants or prostheses as lasting bone substitutes.

The aim of this study is to prepare a nanoparticulate carrier for tunable and sustained delivery of antibiotics following its implantation in the zone of infection. In parallel with the drug release process, the particles would decompose, dissipate their osteogenic contents and thus foster the bone healing process and natural restoration of the portion of bone damaged by the pathogen, avoiding both (a) the long-term repetitive administration of the drug and (b) surgical debridement. In previous studies, we reported on the methods for the formation of calcium phosphate (CAP) and poly-(D,L-lactide-co-glycolide)-coated calcium phosphate (PLGA/CAP) particles loaded with clindamycin phosphate (CL), a broad-range antibiotic commonly prescribed to treat osteomyelitis [7, 8]. We demonstrated that variations in the phase composition of the CAP carriers can be used to tailor the carrier degradation and drug release time scales from hours to weeks to months to a year or more, depending on whether the phase composition corresponded to mono-CAP, di-CAP, amorphous CAP or hydroxyapatite (HAP), respectively. In this work, we report on the results of a comparative analysis of the response of osteblastic cells *in vitro* to the nanoparticulate drug carriers comprising either various CAP phases or PLGA/HAP, alongside their assessment of antibacterial performance against *Staphylococcus aureus*, the main causative agent of osteomyelitis. One such comparative analysis was meant to highlight the extent to which PLGA coatings on the surface of CAP particles interfere with the already verified antimicrobial effect of CL-impregnated CAP powders and their osteoinductive character [9].

2. Experimental

2.1.Synthesis and characterization of clindamycin-impregnated CAP and PLGA/CAP powders

The method for the preparation of HAP was adapted and modified from a previous publication [10]. It began with adding 5 mL of 0.06 M aqueous solution of $NH_4H_2PO_4$ containing 0.3 mL 28 % NH_4OH dropwise (13.3 mL/min) to the same volume of 0.1 M aqueous solution of $Ca(NO_3)_2$ containing 0.6 mL 28 % NH_4OH, vigorously stirred with a magnetic bar (400 rpm) and kept on a plate heated to 50 °C. After the addition of $NH_4H_2PO_4$ was complete, the suspension was brought to boiling, then immediately removed from the heater and let cool in air. Stirring was suspended and the precipitate alongside its parent solution was left to age in atmospheric conditions for 24 h. After the given time, clindamycin phosphate (CL; *Tokyo Chemical Industry*) in the amount of 4.4 mg was added to the suspension and the agitated drugcontaining sol was aged for 5 min. The precipitate was then washed once with deionized (DI) H_2O, centrifuged (10 sec at 3500 rpm), and let dry overnight in a vacuum oven (p = −20 mmHg) at 80 °C.

To synthesize monetite (dicalcium phosphate anhydrous; DCPA, $CaHPO_4$), the same procedure was repeated using 400 mL 0.33 M $Ca(NO_3)_2$ and 400 mL 0.25 M $NH_4H_2PO_4$ containing 10 mL 28 % NH_4OH, with bringing the suspension to boiling afterwards. Amorphous CAP (ACP) was formed by abruptly adding a solution containing 100 mL 0.5 M $Ca(NO_3)_2$ and 7 mL 28 % NH_4OH into a solution comprising 100 mL 0.2 M $NH_4H_2PO_4$ and 4 mL 28 % NH_4OH. The fine precipitate formed upon mixing was aged for 15 s, before it was collected, centrifuged, washed with 0.14 w/v% NH_4OH, centrifuged again, dried overnight at low pressure (p = −20 mmHg) and room temperature, and stored at 4 °C to prevent spontaneous transformation to HAP.

To synthesize monocalcium phosphate monohydrate $(Ca(H_2PO_4)_2 \cdot H_2O$, MCPM), identical volumes of 3.5 M H_3PO_4 (40 wt% conc. H_3PO_4) and 1.8 M $Ca(NO_3)_2$ were mixed and brought to boiling under intensive stirring. The white precipitate formed through evaporation of the solvent was repeatedly alternately centrifuged and washed with ethanol to remove H_3PO_4, separated from the supernatant, dried for 30 min at room temperature and stored at 4 °C to prevent transformation to DCPA. Different CAP phases synthesized and analyzed in this work, along with their solubility rates, are given in Table 1

The method for preparation of PLGA-coated HAP loaded with CL (*Sigma*) was adapted from a previous publication [8]. HAP nanoparticles were ultrasonically dispersed in 10 mL ethanol at c = 10 mg/mL for 10 min and processed using a 700 Watt *Qsonica* sonicator and a 1/8" microtip. This was followed by their centrifugation at 4000 rpm and separation from the liquid medium. PLGA (M_w = 45 – 75 kg/mol; co-monomer ratio 50:50, *Durect*) in the amount of 900 mg was then added to 40 mL of acetonitrile, to which 10 mL of either 9.6 or 19.2 mg/mL aqueous solution of CL were admixed, and cooled down to 8 °C under intensive agitation. The solid pellet of HAP was added to the PLGA/CL solutions and ultrasonically dispersed for 2 min, after which 80 mL H_2O was added to initiate the precipitation of the polymer and formation of the PLGA/HAP composite with encapsulated CL. The resulting suspension was added dropwise to 200 mL of 2 wt% poly-vinyl-pyrrolidone solution in water to stabilize the surface of the particles. Sedimentation was induced by 2 h long centrifugation at 4000 rpm and 8 °C to prevent coalescence of the particles. The precipitated was dried in air.

Overall, drug loading in the case of CAP powders was accomplished by a two-step process consisting of: (a) drug adsorption by aging in the stirred CAP sol; and (b) drying-induced particle aggregation and formation of compact microscopic blocks. In the case of PLGA/

CAP powders, loading of the drug was carried out by capturing the drug within the co-precipitated polymeric shell, in addition to the identical step (a). The amount of the drug added to each CAP powder was normalized to the theoretical yield: $m_{CL}(MCPM) = 8.6m_{CL}(DCPA) = 1.13m_{CL}(ACP) = 5m_{CL}(HAP)$ for identical volumes of $Ca(NO_3)_2$ and $NH_4H_2PO_4$ solutions. In the case of HAP, e.g., it amounted to 4.4 mg per 1 mmol of Ca^{2+} or 44 μg per 1 mg of the powder. As deduced from HPLC analyses (*Hewlett Packard 1050*), the loading efficiency increased 1.5 times when encapsulation of the drug by polymerization was coupled to adsorption.

The solubility measurements were carried out by immersing 10 mg of each CAP powder separately in 10 mL of either 20 mM Tris/HCl (pH 7.4) or 20 mM MES/NaCl (pH 6.0) and periodically reading the concentration of free calcium ions in the solution ($[Ca^{2+}]$) on an Accumet AR15 pH-meter (*Fisher Scientific*) using a Ca^{2+} microelectrode in combination with a reference electrode (*Microelectrodes, Inc.*). The solution was replaced every 24 h to prevent saturation and minimize the effects of spontaneous re-precipitation. The phase composition of the particles was analyzed on a *Bruker AXS D4 Endeavour* X-ray diffractometer using $Cu_{K\alpha} = 1.5418$ Å as the wavelength of the radiation source. The step size was 0.02 °, with 2 s of sample irradiation time per step. The size distribution profiles and morphology of the powders was analyzed using a *Hitachi* S-4300SE/N scanning electron microscope (SEM), a SUPRA 35 VP *Zeiss* field-emission SEM (FE-SEM), as well as a JEOL 3010 transmission electron microscope (TEM) and a JEM-2010F high-resolution TEM (HR-TEM).

2.2. Bacterial studies

The gram-positive bacterium *Staphylococcus aureus* was chosen for our study because it is the most common cause of osteomyelitis [11–12]. A single colony of *Staphylococcus aureus* (ATCC 25923) cultured on a blood agar plate over 48 h was stabbed with a pipette tip, which was then placed in 5 mL of 37 mg/mL brain heart infusion (BHI) broth and kept on an incubator shaker (*Innova 44*) overnight at 37 °C and 225 rpm. To determine the minimal inhibitory concentration (MIC) of the CL-containing particles, the turbid broth was collected the following day and 8 nL of it was added to 1 mL of 37 mg/mL BHI broth (1:125,000 dilution of bacteria) containing different amounts of the particles. The resulting bacterial concentration was determined to be equal to 10^5 bacteria per mL by comparing the optical density at $\lambda = 600$ nm of a range of serially diluted bacterial broths with similarly serially diluted 0.5 M McFarland solution (equivalent to approximately 10^8 bacteria per mL) prepared by mixing 1 % $BaCl_2$ solution and 1 % H_2SO_4 in the volume ratio of 1:200. The CL-containing particle/bacterial samples were incubated overnight on the incubator shaker and their turbidity, the indicator of bacterial concentration, was assessed the following day. Parallel bacterial studies were carried out on sheep blood agar plates (UCSF Cell Culture Facility) using a modified Kirby-Bauer method for antibiotic testing. A freshly inoculated bacterial broth was diluted to the concentration of 10^8 colony forming units per mL and 200 μL of it were added to the plate and spread so as to fully cover the surface. Five milligrams of the particles were then added onto the plate in form of separate islets. The control plate was seeded with the same bacterial concentration, after which CL-free silica beads, HAP, PLGA and PLGA/HAP were added to it. The plates were incubated overnight at 37 °C and observed for inhibition of bacterial growth around the nanoparticle samples the following day. All the particle types were analyzed in triplicates.

2.3. Cell culture studies

Mouse calvarial preosteoblastic cell line, MC3T3-E1 subclone 4, was purchased from American Tissue Culture Collection (*ATCC*, Rockville, MD) and cultured in Alpha Minimum Essential Medium (α-MEM; *Gibco*) supplemented with 10% fetal bovine serum

(FBS, *Invitrogen*) and no ascorbic acid (AA). The medium was replaced every 48 h, and the cultures were incubated at 37 °C in a humidified atmosphere containing 5% CO_2. Every 7 days, the cells were detached from the surface of the 75 cm^2 cell culture flask (*Greiner Bio-One*) using 0.25 wt% trypsin, washed, centrifuged (1000 rpm × 3 min), resuspended in 10 mL α-MEM and subcultured in 1:7 volume ratio. Cell passages 2 – 7 were used for the experiments reported hereby. In all experiments, the cells were seeded either in 96 well plates and 100 μL of media at a density of 10^4 cells per well or on glass cover slips placed in 24 well plates and 400 μL of media at a density of $6 \cdot 10^4$ cells per well. The cultures were regularly examined under an optical microscope to monitor growth and possible contamination. Near confluence, cells were treated with 2 mg/cm^2 of CL-containing CAP or PLGA/CAP particles and 50 μg/mL AA as the mineralization inductor, and incubated for 7 – 10 days. Alpha-MEM supplemented with 50 μg/mL AA was replenished every 48 h. Cells incubated with pure CL were cultured in the same medium containing 100 μg/mL CL.

After 1 – 3 weeks of incubation in the presence of the drug-containing particles, cells grown in 24 well plates were stained for collagen type I, f-actin and nucleus. The staining procedure began with washing the cells with phosphate buffer saline (PBS; pH 7.4) and fixing them for 15 min in 3.7 % paraformaldehyde. The cells were then washed with PBS 3 × 5 min and then with the blocking solution (PBT = 1 % Bovine Serum Albumin (BSA), 0.1 % Triton X-100 in PBS) 2 × 5 min. The cells were then blocked and permeabilized in PBT for 1 h. In the case of staining for collagen, the cells were then incubated with 100 μL/well of the primary antibody, 10 μg/mL rabbit anti-collagen-type-1 (*Abcam*) in PBT for 1 h. The cells were then washed with PBS 3 × 10 min and incubated with 100 μL/well of the secondary antibody, 10 μg/mL AlexaFluor 555 goat anti-rabbit IgG (Invitrogen) and 20 μg/mL 4',6-diamidino-2-phenylindole dihydrochloride nuclear counterstain (DAPI, Invitrogen), all in PBT for one hour and then washed with PBS 3 × 5 min. The DAPI/secondary-antibody solution also contained either 2 μM calcein AM as CAP particle-staining compound or 20 μg/mL FITC-BSA as a nonspecific polymer-staining compound. In the case of staining for f-actin, the cells were incubated with 100 μL/well of 10 μg/mL phalloidin-tetramethylrhodamine (AlexaFluor 555, Invitrogen) and 20 μg/mL DAPI, all in PBT for one hour and then washed with PBS 3 × 5 min. The cover slips containing the fixed and stained cells were mounted onto glass slides using hard set vectashield and nail polish and were subsequently imaged on a confocal laser scanning microscope – C1si (UCSF Nikon Imaging Center) at 20 – 100× magnification in oil. All the experiments were done in triplicates. To assess the live/dead ratio of cells incubated with the antibiotic-containing particles, *Invitrogen* L-3224 live/dead assay was carried out. It involved staining the cells after different incubation times with 2 μM calcein AM and 4 μM ethidium homodimer-1 (EthD-1) in PBS and incubating at 37 °C for 45 min. Inverted cover slips containing cells and CAP/CL particles were then mounted on microscope slides wetted with 20 μL of the staining solution and sealed using nail polish. Immediately thereafter, the live/dead cell count was performed under an *Olympus BX60* optical microscope at 20× magnification.

After the incubation period of 10 days, cell lysis, reverse transcription (*Bio-Rad*) and qPCR (*Applied Biosystems, StepONEPlus*) were performed using the Fast SYBR Green Cells-to-CT kit (*Ambion*) in accordance with the manufacturer's instructions. Each experiment was done in quadruplicates, while each experimental replica was analyzed for mRNA expression in triplicates (n = 4 × 3). The expressions of one housekeeping gene, β-actin (*ACTB*), and five osteogenic markers, mouse type I procollagen (*Col I*), alkaline phosphatase (*ALP*), osteocalcin (*BGLAP*), osteopontin (*BSP-1*) and *Runx2* were analyzed. The following primer pair sequences were used [13–15]: *ACTB* forward 5'-GGCCCAGAGCAAGAGAGGTATCC-3', reverse 5'-ACGCACGATTTCCCTCTCAGC-3'; *Col I* forward 5'-GCGAAGGCAACAGTCGCT-3', reverse 5'-CTTGGTGGTTTTGTATTCGATGAC-3'; *ALP* forward 5'-

TCCTGACCAAAAACCTCAAAGG-3', reverse 5'-TGCTTCATGCAGAGCCTGC-3'; *BGLAP* forward 5'-CTCACAGATGCCAAGCCCA-3', reverse 5'-CCAAGGTAGCGCCGGAGTCT-3'; *BSP-1* forward 5'-AGGAGGAGGCAGAGCACA-3', reverse 5'-CTGGTATGGCACAGGTGATG-3'; *Runx2* forward 5'-AAATGCCTCCGCTGTTATGAA-3', reverse 5'-GCTCCGGCCCACAAATCT-3'. The real-time PCR results were analyzed using the $\Delta\Delta C_t$ method [16] and all the data were normalized to *ACTB* expression levels.

For the purpose of MTT (3-[4, 5-dimethylthiazol-2-yl]-2, 5-diphenyl tetrazolium bromide) *in vitro* toxicological assay, MC3T3-E1 fibroblasts were seeded in 48 well plates at the density of $3 \cdot 10^4$ cells per well and cultured in FBS-supplemented α-MEM without AA. Upon seeding, different ceramic and polymeric powders, with and without CL, were added to the cells. Cells incubated with CL only were cultured in media supplemented with 100 μg/mL CL. The incubation lasted for 96 h and the media were replenished once, in the middle of the incubation period. At the end of 96 h, 20 μL of 5 mg/mL MTT (*Sigma M-5655*) in PBS were added to each well already containing 200 μL of media. Following 2 h incubation at 37 °C, 220 μL of MTT solubilization solution (*Sigma M-5655*) were added to each well. The plate was shaken at room temperature for an hour and samples from each well were analyzed for absorbance at 570 nm on a UV/Vis spectrophotometric microplate reader (*Molecular Devices: Spectra Max 190*). All the particle types were analyzed in biological triplicates and the resulting absorbance values were normalized to the negative control.

3. Results and discussion

3.1. Morphological and structural characterization

Results of the morphological analysis of HAP and PLGA/HAP particles loaded with CL are shown in Figs.1–2. Both types of particles are of spherical shape and their sizes are in the range of 20 – 60 nm (Fig.1) and 100 – 300 nm (Fig.2a–c), respectively. HR-TEM analysis has revealed that the narrowly dispersed composite particles loaded with CL (Fig.2a–c) comprise a polymeric shell coated around nanosized HAP particles (Fig.2d–e) and has also provided an insight into the nonporous interface between PLGA and HAP (Fig.2f). While efficient loading of CL within HAP powders was contingent upon the physisorption of the drug and desiccation-controlled aggregation of individual nanosized particles, PLGA/CAP spheres exhibited an equally strong tendency towards the formation of flaky aggregates, even though the drug was loaded onto them mainly via co-precipitation with the polymer. Despite the aggregation, both types of particles resisted coalescence and preserved their individual nature.

The structural analysis of the powders by means of X-ray diffraction (XRD), the results of which are displayed in Fig.3, demonstrates that most CAP particles were covered with PLGA during the encapsulation process, as evident from the effect of increased amorphousness that PLGA has on the XRD pattern of pure HAP. Diminished intensity of HAP diffraction peaks in CL-containing PLGA/HAP compared to those in unloaded PLGA/HAP also demonstrates that formerly adsorbed CL increases the efficiency of encapsulation of HAP particles within PLGA by acting as a surface interaction mediator. HAP co-precipitated with CL also exhibits broader diffraction peaks indicative of lower crystallinity, furthermore proving the surface active role of CL as well as its ability to moderately strongly adsorb onto CAP.

3.2. Solubility and drug release

Normalizing the measured amount of Ca^{2+} ions released into the solution by different monophasic CAP powders (Fig.4) has indicated that different CAP phases dissolve at a

different rate, ranging from 1–2 h for MCPM to 1 week for DCPA to 3 months for ACP to a year for HAP at pH 7.4 under daily replacements of the solution and 1 mg/mL concentration of the powder. At pH 6.0, the only change in the solubility profile, the kinetic factor directly coupled to the drug release rate, was observed for the acidic DCPA whose stability period in the solution increased to 2–3 weeks and for ACP which dissolved under the given conditions one-third faster than at pH 7.4, that is, in 3 months, a natural consequence of the acidic nature of the former ($CaHPO_4$) and the alkaline nature of the latter ($Ca_3(PO_4)_2 \cdot nH_2O$; $pK_{b1}(Ca(OH)_2) = 2.4 < pK_{a2}(H_3PO_4) = 7.2$). This difference in solubility between different CAP powders could be predicted from their solubility products: namely, theoretical pK_{sp} equals 1, 7, 25 and 117 for MCPM, DCPA, ACP and HAP, respectively (Table 1).

Drug release profiles were presented in earlier reports [17, 18], showing 68 wt% of CL released in a month from PLGA/HAP particles and only 0.5 wt% released in the first 24 h. In contrast, the drug desorption from HAP surface followed burst release profile with about 30 % of the drug being released in the first 24 h. In terms of absolute amounts, the comparative release profiles are displayed in Fig.5, showing a more abrupt release from HAP powders due to desorption effect and a more sustained subsequent release driven mostly by the concentration gradient caused by the daily replacement of the medium. On the contrary, the released amount of CL from PLGA/HAP spheres is relatively small in the first 5 days, but is accompanied by a rather rapid release between days 7 and 10 when the swelling-induced erosion of the polymer becomes significant and the small drug is free to diffuse out through the open pores [19]. Unlike the delivery of many non-antibiotic therapeutic agents whereby burst release is considered undesirable and zero-order release kinetics is thought of as ideal, the effective delivery of antibiotics crucially depends on the ability of carriers to release a certain amount of the drug abruptly, during the first 24 h, so as to exceed the MIC for the given bacterial population and suppress its growth, lest it become potentially resistant to the antibiotic should this initial release be below the MIC level. The design of optimal drug release profiles for antibiotics is consequently focused on a comparatively shorter time scale than for non-antibiotic compounds, with the largest emphasis on the first week following surgical implantation of the carrier. Since six weeks comprises the typical long-term antibiotic therapy against inflamed bone tissue, the small molecule drug release profile displayed by HAP in Fig.5 seems promising.

The release of CL from CAP and PLGA/CAP particles proceeds governed by two distinct kinetic mechanisms: solubility of the carrier in the former and hydration-induced degradation of the polymeric shell in the latter case, alongside desorption from the carrier surface somewhat present for both particles. To compare their drug delivery efficacy, a parallel antibacterial assessment was performed. As shown in Fig.6a, considerably large inhibition zones were visible following an overnight incubation of all the CL-containing particles on blood agar plates seeded with $7 \cdot 10^3$ *Staphylococcus aureus* bacteria per mm^2. In contrast, all of the CL-free control samples, including HAP, PLGA/HAP, PLGA and silica beads, were covered with bacterial colonies (Fig.6b), indicating that inhibition is due to the antibiotic and not the carrier. Incubation of CL-comprising particles under more dynamic conditions that involved 225 rpm shaking at 37 °C and the initial bacterial concentration of 10^5/mL of the broth led to an equally effective bacteriostatic performance of the particles, as shown in Fig.7. Since the degradation of both types of particles and the corresponding drug release are expected to be considerably slower on agar plates than in shaken broths, comparatively large inhibition zones formed around the particles suggest the presence of a certain amount of the drug on the particle surface.

3.3. Bacterial studies

Although a low-pH microenvironment has been shown to lead to a multiple-fold increase in the MIC against *Staphylococcus aureus* and acidic products of PLGA degradation [20, 21]

could have a chance to reiterate such an unfavorable effect (unlike the two alkaline forms of CAP used in this study: HAP and ACP), both types of particles were shown to be effective in inhibiting bacterial growth in broths as well as in forming relatively large bacteria-free zones on blood agar plates. The amount of the particles required to suppress the bacterial growth correlates well with the encapsulated amounts of CL shown in Table 2. The greater the amount of loaded CL within PLGA/HAP powders, the lower the MIC. Despite the fact that HAP/CL powder relies on sheer adsorption effects to capture the drug - together with the subsequent entrapment of the drug within large microparticles as a result of the desiccation process - it has exhibited an equally effective ability to eradicate the source of infection as particles encapsulating the drug within a more protective polymeric shell. Encapsulation of CL within the polymeric particles still markedly extended the antibiotic half-life upon storage at room temperature, as PLGA/HAP/CL nanoparticles did not show diminished antibiotic activity even after two years of storage.

3.4. Immunofluorescent staining

In our earlier study [9] we witnessed diminished osteogenic activity of osteoblastic cells cultured with a moderate concentration of CL (100 μg/mL). However, when incorporated within CAP carriers, this unfavorable effect was compensated for by the osteogenic potential of the former, while the antimicrobial properties of drug-containing powders were retained. The results obtained on cell cultures in this work corroborate these findings by demonstrating a viable response of osteoblastic cells to all types of CL-containing particles. In-plane and z-stacked confocal optical micrographs, the results of fluorescent staining of CAP/CL and PLGA/HAP particles and osteoblastic cells after 7 – 21 days of incubation in differentiation medium, are shown in Figs.8–14. Cells are shown adhered and spread on practically all CAP/CL microparticles composed of smaller, nanosized units. Blue-stained cell nucleus is correspondingly observed elongated in the direction of the particle surface, while red-stained factin cytoskeleton of confluent cells typically fully enwraps the particle surface (Figs.8, 10a, 12). The intimate interaction between the cells and the particles, being a direct morphological indicator of the surface's osteoconductivity [22], was evidenced for all the sparsely soluble CAP phases, with or without loaded CL: HAP, ACP and DCPA (Figs.8, 9, 12). No significant difference in cell response to CAP particles was observed depending on whether the incubation lasted for 7, 10 or 21 days. Also, intact, striated cytoskeletal pattern was detected for both the negative control, incubated without any particles, and cells incubated in the presence of any of the CL-containing CAP powders (Fig.11).

One of the main differences observed between different CAP phases was that the detachment of smaller CAP particle islands from bigger, microsized blocks of CAP onto which cells facilely adhered was more present among more soluble DCPA and ACP compared to the least soluble HAP (Fig.8, 9). The smaller fluorescent particles were typically observed in the direct vicinity of larger CAP blocks, indicating that they have detached from them during the dissolution process, presumably facilitated by the cell binding and spreading. The smaller CAP particles were, however, not discernable from the mineral particles produced by osteoblastic cells during their formation of the extracellular matrix (EM), a process which takes 7 – 10 days for the given cell clone. The amount of small mineral particles dispersed across the cell surface increased with the incubation time and for DCPA, the only phase that fully dissolves itself in about 2–4 weeks when the medium is replaced every 48 h at the standard concentration of 1 mg/mL, this meant gradual disappearance of large microscopic blocks when the incubation time was extended to maximal 21 days (Fig.9). For this CAP phase, therefore, the only mineralized content of the stained samples after 3 weeks of incubation time corresponded to small particulate remnants of the dissolution process, indistinguishable from the mineralized EM formed by the cells (Fig.13), as opposed to microscopic HAP and ACP particle conglomerates still present to a

great extent after 21 days. The tendency of more soluble ACP and especially DCPA conglomerates to lose their integrity and gradually dissolve or redisperse their nanoparticulate and drug contents was evident during confocal imaging (Figs.8–9). Namely, while microscopic HAP blocks demonstrate well defined borders and uniformity in fluorescence, this does not hold for DCPA and ACP, for which the light intensity appears more dissipated, indicating faster biodegradation.

Cells have demonstrated equally favorable adherence and spreading on PLGA/HAP particle conglomerates as on CAP. Staining of PLGA surface was less effective than that of CAP surface due to the presence of poly-vinyl-pyrrolidone molecules that protected the particles from coalescence during the preparation stage. The degradation products of PLGA *per se* are safe as they become isolated from the organism as routine fermentation end-products. The degradation of PLGA, however, produces a local drop in the pH [23] and this acidification effect can lead to increased hard tissue resorption and bone mass loss [24, 25]. Chronic inflammation is known to often result as a response to implantation of poly-lactic-acid-based polymers in bone tissue engineering [26–28]. However, impregnation of the pure acidic polymer with bone morphogenetic proteins has been shown to overcome the inflammatory response and induce full bioresorption of the polymer and enhance bone growth [29–31]. Similarly, the addition of demineralized bone particles to PLGA was shown to lessen the inflammation in the vicinity of PLGA and reduce the fibrous tissue encapsulation and foreign body giant cell response [32]. The same effect of increased biocompatibility of PLGA was observed upon admixing an antibiotic, tetracycline, to it [33]. The buffered media, the mild dissolution of alkaline HAP and the slow degradation of PLGA, likewise, mitigate the acidifying effect of sole PLGA dissolution and render the particles "likable" to the cells. As shown in our previous study, the relatively quick dissolution of the most acidic CAP phase, MCPM, is sufficient to completely wipe out the cell population unless it becomes promptly aspirated and replenished with fresh media immediately following its 1 h dissolution.

Cells found in close contact with both the polymeric and CAP surfaces and live/dead ratio in excess of 98 % for all the CL-containing particles have suggested no toxic effects of any of the particles on the cells. The used cell line, MC3T3-E1 subclone 4, is known to form a fully mineralized EM after 7 – 10 days of incubation in the differentiation medium and the addition of any of the CL-containing particles at the onset of initiated differentiation to osteoblastic phenotype did not interfere with the capacity of cells to form the EM. This was evidenced by biomineral particles being formed in all cell samples, including the negative control (Fig.13), as well as by an equal density of collagen matrix built by the cells incubated in the presence of any of the drug-loaded particles and the negative control (Fig. 14). In terms of the intensity of fluorescence from fluorophore-tagged collagen type I, no significant difference existed between the control and any of CAP or PLGA/HAP samples with or without CL. As for fluorescent mineral particles, higher fluorescence intensity was detected from samples incubated with CAPs, partly owing to the very drug-containing particles initially added to the cultured cells (Fig.13).

3.5. Gene expression analysis and cell viability assay

The results of the gene expression analysis of the effects of various HAP/CL and PLGA/ HAP/CL powders on osteoblastic MC3T3-E1 cells are displayed in Fig.15. Transcription levels of osteogenic markers *BGLAP, Col I* and *Runx2* were all significantly elevated with respect to the negative control. *BGLAP* is a gene encoding for osteocalcin, a protein that is a potent promoter of nucleation of biominerals that constitute the EM formed by the osteoblastic cells; *Col I* codes for protocollagen type I, a precursor of the most prevalent form of collagen, another essential constituent of the EM; *Runx2* is a key transcription factor for osteoblast differentiation. Therefore, these results unequivocally suggest that both types

of antibiotic-loaded particles have the ability to enhance the mineralization activity of the cell phenotype. In our previous work [9], we noticed that the addition of pure CL to cell growth media in a similar amount as that released by the given particles leads to significant, multiple-fold downregulation of the same three osteogenic markers. The MTT assay, the results of which are given in Fig.16, however, showed no negative effects on pre-osteoblast cell proliferation of either CL alone or any of the CL-loaded particles, suggesting that the negative effects of CL are limited to reducing the osteogenic activity of bone cells. The mild decrease in the amount of mitochondrial dehydrogenases, directly proportional to the cell number, for CL-loaded CAP particles was attributed to visually detected binding of the colorimetric agent to CAP crystals. Both CL-loaded HAP and PLGA/HAP, however, have the ability to compensate for the negative effect of the pure antibiotic. This is consistent with the previously detected ability of HAP and its ionic degradation products to upregulate specific osteogenic markers [34–36]. Coupled to each other within composite particles, the antimicrobial CL and osteogenic CAP or PLGA/HAP provide for a synergy that complements each other's positive effects, while annulling the negative effects that pure CL and other antibiotics impregnated within bone cements have been evidenced to exert on the osteogenic activity of osteoblastic cells [37–39].

The upregulation of more ambiguous osteogenic markers, BSP-1 and ALP, was less clear and significant only for PLGA/HAP and BSP-1. This is partly expected since *ALP* upregulation is associated not only with the new bone growth [40], but also with multiple other metabolic processes in both differentiated and undifferentiated fibroblasts. *BSP-1*, on the other hand, encodes for osteopontin, the protein that acts as a mineralization inhibitor rather than promoter, as *BGLAP* does. It is also a negative regulator of proliferation and differentiation in MC3T3-E1 cells [41], explaining for the less evident effects of osteogenic HAP and PLGA/HAP on its expression levels. The latter were 100–200 times lower than those of the housekeeping gene, *ACTB*, generally a good sign for the viability of the cell population. The same is indicated by the multiple-fold increase in the expression of BGLAP; by comparatively low expression of *ALP*; and, in particular, by approximately 400 times more elevated expression of *Col I*, all with respect to *ACTB*.

4. Conclusion

Performed was a comparative analysis of the antibacterial activity and *in vitro* response of osteoblastic cells to two types of calcium-phosphate-based antibiotic carriers - with and without poly-(D,L-lactide-co-glycolide) coating - potentially applicable in the treatment of osteomyelitis. Both calcium phosphate particles of different phases and solubility/drug-release time scales, ranging from a week to 3 months to a year, and core-shell composites comprising hydroxyapatite nanoparticles encapsulated within a poly-lactide-co-glycolide shell induced a positive response by the osteoblast-like cells in the course of incubation that lasted for up to three weeks. They were also highly effective in suppressing the growth of *Staphylococcus aureus*, the main causative agent of osteomyelitis, in both broth and agar cultures. Neither the pure antibiotic utilized in this study, clindamycin phosphate, nor any of the drug carriers, with or without the encapsulated drug, were shown to exert cytostatic or cytotoxic effects on the osteoblastic cells. Clindamycin phosphate at the moderate concentration of 0.1 mg/mL was, however, shown in an earlier study to downregulate the gene expression of multiple osteogenic markers. Real-time PCR analysis carried out in this work demonstrated the ability of both types of calciumphosphate-based drug carriers to compensate for the negative effects of the pure antibiotic by means of their intrinsic osteogenic nature. The drug-containing carriers were thus shown to upregulate the expression of four potent osteogenic markers osteocalcin, osteopontin, Runx2 and protocollagen type I, suggesting their ability to promote osteogenesis and enhance remineralization of the infected site, alongside eliminating the bacterial source of infection.

Our future direction of research will aim at further enhancing the osteogenic response of osteoblastic cells to the antibiotic-loaded particles using bone growth factors. Their sustained release has been considered of critical importance in making the material osteoinductive [42], just about as much as the prolonged release of the time-dependent antibiotic utilized in this study, clindamycin phosphate, was shown as vital in preventing it from lowering the osteogenic potential of bone cells, while still exceeding the critical levels required for it to act in an effective bacteriostatic manner. Optimization of the particle morphology, e.g., substituting spherical calcium phosphate particles with plate-shaped, bone-like ones, was also shown to be a crucial step in endowing calcium phosphates with favorable osteopromotion capacities [43]. The corresponding optimization of the particle morphology will present another future direction of our research.

Acknowledgments

References

1. Del Pozo JL, Patel R. New Eng. J. Med. 2009; 361:787–794. [PubMed: 19692690]

2. Baltensperger, MM.; Eyrich, GK., editors. Osteomyelitis of the Jaws. Berlin: Springer-Verlag; 2009.

3. Krakowiak PA. Oral Maxillofac. Surg. Clin. North Am. 2011; 23:401–413. [PubMed: 21798440]

4. Humber CC, Albilia JB, Rottenberg B. J. Can. Dent. Assoc. 2011; 77:b98. [PubMed: 21810374]

5. Yenson A, de Fries HO, Deeb ZE. Otolaryngol. Head Neck Surg. 1983; 91:173–176. [PubMed: 6408574]

6. Hatzenbuehler J, Pulling TJ. Am. Fam. Physician. 2011; 84:1027–1033. [PubMed: 22046943]

7. Uskokovi V, Desai TA. J. Biomed. Mat. Res. A. 2013 in press.

8. Vukomanovi M, Škapin S, Jan ar B, Maksin T, Ignjatovi N, Uskokovi V, Uskokovi D. Coll. Surf. B Biointer. 2011; 82:404–413.

9. Uskokovi V, Desai TA. J. Biomed. Mat. Res. A. 2013 in press.

10. Markovi S, Veselinovi Lj, Luki M, Karanovi Lj, Bra ko I, Ignjatovi N, Uskokovi D. Biomed. Mat. 2011; 6:045005.

11. Mruk AL, Record KE. Orthopedics. 2012; 35:401–407. [PubMed: 22588396]

12. Montanaro L, Testoni F, Poggi A, Visai L, Speziale P, Arciola CR. Int. J. Artif. Organs. 2011; 34:781–788. [PubMed: 22094557]

13. Kim SW, Her SJ, Park SJ, Kim D, Park KS, Lee HK, Han BH, Kim MS, Shin CS, Kim SY. Bone. 2005; 37:359–369. [PubMed: 15978880]

14. Rousseau M, Boulzaguet H, Biagianti J, Duplat D, Milet C, Lopez E, Bedouet L. J. Biomed. Mat. Res. A. 2007; 85:487–497.

15. Celetti A, Testa D, Staibano S, Merolla F, Guarino V, Castellone MD, Iovine R, Mansueto G, Somma P, De Rosa G, Galli V, Melillo RM, Santoro M. Clin. Cancer Res. 2005; 11:8019–8027. [PubMed: 16299231]

16. Pfaffl MW. Nucl. Acid. Res. 2001; 29:e45.

17. Vukomanovi M, Škapin SD, Poljanšek I, Žagar E, Kralj B, Ignjatovi N, Uskokovi D. Coll. Surf. B: Bioint. 2011; 82:414–421.

18. Vukomanovi M, Zavašnik-Bergant T, Bra ko I, Radmilovi V, Davor Škapin S, Ignjatovi N, Uskokovi D. Coll. Surf. B: Bioint. 2011; 87:226–235.

19. Lemaire V, Bélair J, Hildgen P. Int. J. Pharm. 2003; 258:95–107. [PubMed: 12753757]

20. Vey E, Roger C, Meehan L, Booth J, Claybourn M, Miller AF, Saiani A. Polym. Degrad. Stab. 2008; 93:1869–1876.

21. Kang J, Schwendeman SP. Biomat. 2002; 23:239–245.

22. Haders DJ, Kazanecki CC, Denhardt DT, Riman RE. J. Mater. Sci. Mater. Med. 2010; 21:1531–1542. [PubMed: 20232236]

23. Siepmann J, Elkharraz K, Siepmann F, Klose D. Biomacromol. 2005; 6:2312–2319.

24. Bostman OM. J. Bone Joint Surg. 1991; 73:679–682.

25. Bostman O, Hirvensalo E, Mikinen J, Rokkanen P. J. Bone Joint Surg. 1990; 72:592–596.

26. Solheim E, Sudmann B, Bang G, Sudmann E. J. Biomed. Mater. Res. 2000; 49:257–263. [PubMed: 10571914]

27. Tiainen J, Soini Y, Suokas E, Veiranto M, Törmälä P, Waris T, Ashammakhi N. J. Mater. Sci. Mater. Med. 2006; 17:1315–1322. [PubMed: 17143763]

28. Plachokova A, Link D, van den Dolder J, van den Beucken J, Jansen J. J. Tissue Eng. Regen. Med. 2007; 1:457–464. [PubMed: 18265419]

29. Miki T, Imai Y. Int. J. Oral Maxillofac. Surg. 1996; 25:402–406. [PubMed: 8961028]

30. Jensen T, Baas J, Dolathshahi-Pirouz A, Jacobsen T, Singh G, Nygaard JV, Foss M, Bechtold J, Bünger C, Besenbacher F, Søballe K. J. Biomed. Mater. Res. A. 2011; 99:94–101. [PubMed: 21800419]

31. Ji Y, Xu GP, Zhang ZP, Xia JJ, Yan JL, Pan SH. Ann. Biomed. Eng. 2010; 38:632–639. [PubMed: 20049636]

32. Yoon SJ, Kim SH, Ha HJ, Ko YK, So JW, Kim MS, Yang YI, Khang G, Rhee JM, Lee HB. Tissue Eng. Part A. 2008; 14:539–547. [PubMed: 18352826]

33. Pataro AL, Oliveira MF, Teixeira KI, Turchetti-Maia RM, Lopes MT, Wykrota FH, Sinisterra RD, Cortés ME. Int. J. Pharm. 2006; 336:75–81. [PubMed: 17174495]

34. Rupani A, Hidalgo-Bastida LA, Rutten F, Dent A, Turner I, Cartmell S. J. Biomed. Mater. Res. A. 2012; 100:1089–1096. [PubMed: 22318934]

35. Gabusi E, Manferdini C, Grassi F, Piacentini A, Cattini L, Filardo G, Lambertini E, Piva R, Zini N, Facchini A, Lisignoli G. J. Cell. Phys. 2012; 227:3151–3161.

36. Müller P, Bulnheim U, Diener A, Lüthen F, Teller M, Klinkenberg ED, Neumann HG, Nebe B, Liebold A, Steinhoff G, Rychly J. J. Cell. Mol. Med. 2008; 12:281–291. [PubMed: 18366455]

37. Naal FD, Salzmann GM, von Knoch F, Tuebel J, Diehl P, Gradinger R, Schauwecker J. Arch. Orthop. Trauma Surg. 2008; 128:317–323. [PubMed: 18196254]

38. Antoci V Jr, Adams CS, Hickok NJ, Shapiro IM, Parvizi J. Clin. Orthop. Relat. Res. 2007; 462:200–206. [PubMed: 17572634]

39. Cover NF, Lai-Yuen S, Parsons AK, Kumar A. Int. J. Nanomed. 2012; 7:2411–2419.

40. Xu L, Lv K, Zhang W, Zhang X, Jiang X, Zhang F. J. Mater. Sci. Mater. Med. 2012; 23:1073–1084. [PubMed: 22311076]

41. Huang W, Carlsen B, Rudkin G, Berry M, Ishida K, Yamaguchi DT, Miller TA. Bone. 2004; 34:799–808. [PubMed: 15121011]

42. Mistry AS, Mikos AG. Adv. Biochem. Engin./Biotechnol. 2005; 94:1–22.

43. Tan YF, Hong SF, Wang XL, Lu J, Wang H, Zhang XD. J. Mater. Sci. Mater. Med. 2007; 18:2237–2241. [PubMed: 17597361]

Highlights

- Analyzed were the antibacterial activity and osteoblastic response to calcium-phosphate-based antibiotic carriers with and without poly-lactide-co-glycolide coating.

- The sparsely soluble calcium phosphate phases analyzed included monetite, amorphous calcium phosphate and hydroxyapatite.

- Both types of particles induced a positive response by the osteoblast-like cells and effectively eradicated the source of infection: *Staphylococcus aureus*.

- The drug-containing carriers upregulated the expression of four osteogenic markers, suggesting their ability to promote osteogenesis at the infected site.

Fig.1.
SEM (a) and TEM (b) images of as-precipitated nanospheres of CAP forming compact microscopic blocks and capturing the adsorbed drug upon desiccation.

Fig.2.
FE-SEM (a–c) and HR-TEM (d–f) micrographs of PLGA/HAP/CL powders.

Fig.3.
Normalized X-ray diffractograms of different components of PLGA/HAP/CL powders in
various combinations thereof and alone.

Fig.4.
Cumulative increase in the concentration of Ca^{2+} ions in the supernatant over time, directly indicative of the solubility of the compound, during incubation of 1 mg/mL CAP powder in 20 mM Tris/HCl or MES/HCl buffer and daily replacements of the solution for four different CAP phases, at pHs 7.4 (a) and 6.0 (b).

Fig.5.
A comparative drug release profile for a small organic model drug from the powder obtained by desiccation-induced aggregation of HAP nanoparticles (-○-) and PLGA/HAP powder (-●-). Note that different drug release measurement settings were employed for the two powders: a standard estimation of the release rate from polymeric particles in static solutions for PLGA/HAP and an assessment involving daily replacements of the solvent in the case of sparsely soluble HAP.

Fig.6.
(a) Inhibition zones formed around CL-loaded CAP particles of various monophasic compositions and PLGA/HAP particles encapsulating different amounts of CL (1 and 5 wt %) on sheep blood agar plates seeded with $7 \cdot 10^3$ *Staphylococcus aureus* bacteria per mm^2 following an overnight incubation; (b) no inhibition zones formed around various control samples: silica beads, HAP, PLGA and PLGA/HAP, none of which contained CL.
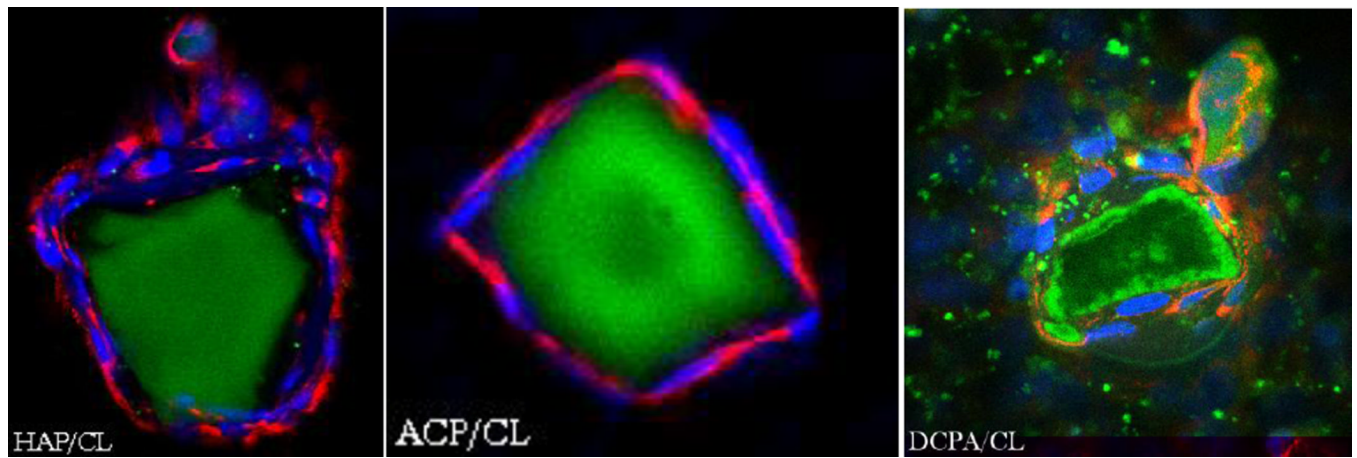
Fig.7.
Visual appearance of turbid/infected and clear/disinfected BHI broths inoculated with *Staphylococcus aureus* (10^5 bacteria per mL) and different amounts of CAP powder loaded with CL, following 24 h incubation.

Fig.8.
Single plane confocal optical micrographs of fluorescently stained DCPA/CL, ACP/CL and HAP/CL particles (green) and osteoblastic MC3T3-E1 cells (cytoskeletal f-actin - red; nucleus - blue) following 7 days of incubation in differentiation medium. The sizes of the images are 270×270 μm.

Fig.9.
Single plane confocal optical micrographs of fluorescently stained HAP/CL, ACP/CL and DCPA/CL particles (green) and osteoblastic MC3T3-E1 cells (collagen type I - red; nucleus - blue) following 21 days of incubation in differentiation medium. The sizes of the images are 675×675 μm (HAP/CL, ACP/CL) and 270×270 μm (DCPA/CL).

Fig.10.
Single plane confocal optical micrographs of fluorescently stained osteoblastic MC3T3-E1 cells incubated with PLGA/HAP/CL for 10 days and stained for nucleus (blue), PLGA (green), (a) cytoskeletal f-actin (red), and (b) collagen type I. The sizes of the images are 675 × 675 μm.
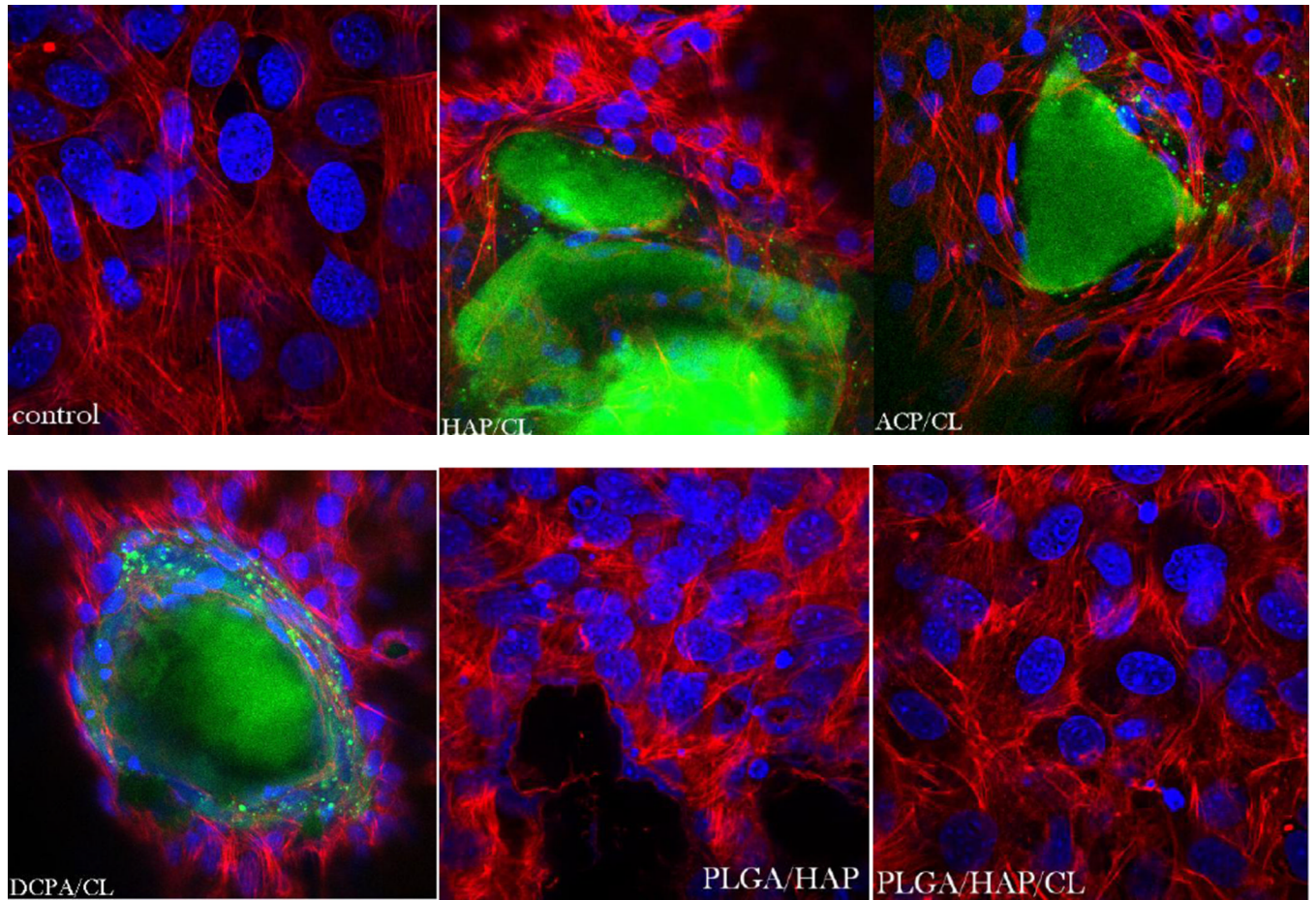
Fig.11.
Single-plane confocal optical micrographs of fluorescently stained osteoblastic MC3T3-E1 cells (cytoskeletal f-actin - red; nucleus - blue) of the control sample and of those incubated with DCPA/CL, HAP/CL, ACP/CL (green), PLGA/HAP (black), and PLGA/HAP/CL, following 10 days of incubation. The sizes of the images are 270×270 μm.

Fig.12.
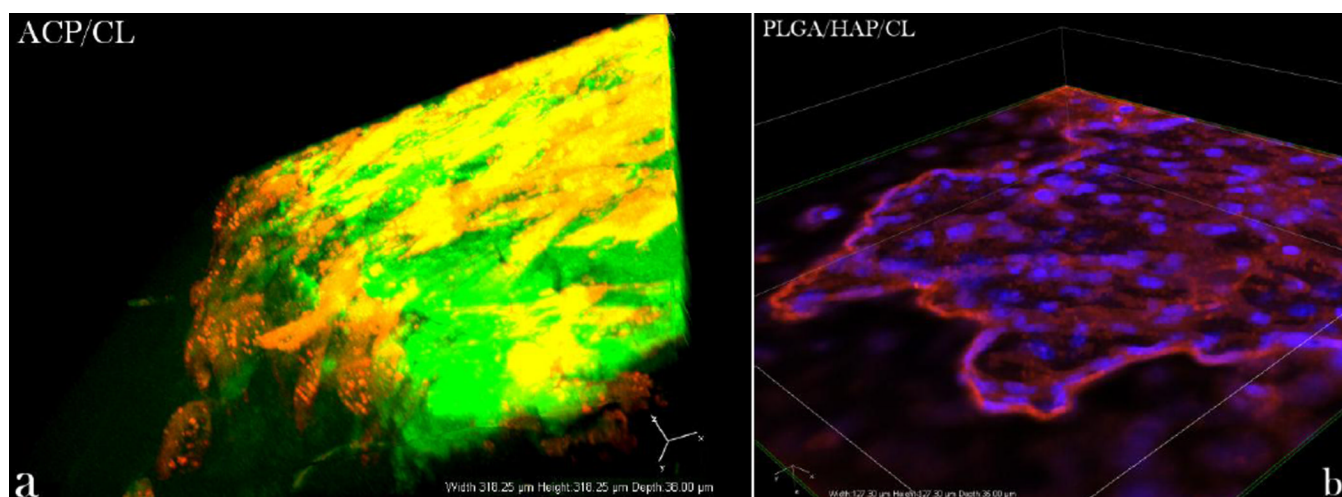3D confocal projections of (a) osteoblast-like cells (red) spread over the surface of CL-containing ACP (green) and (b) osteoblastic-like cells (cytoskeletal f-actin - red; nucleus - blue) spread on top of and around CLcontaining PLGA/HAP.
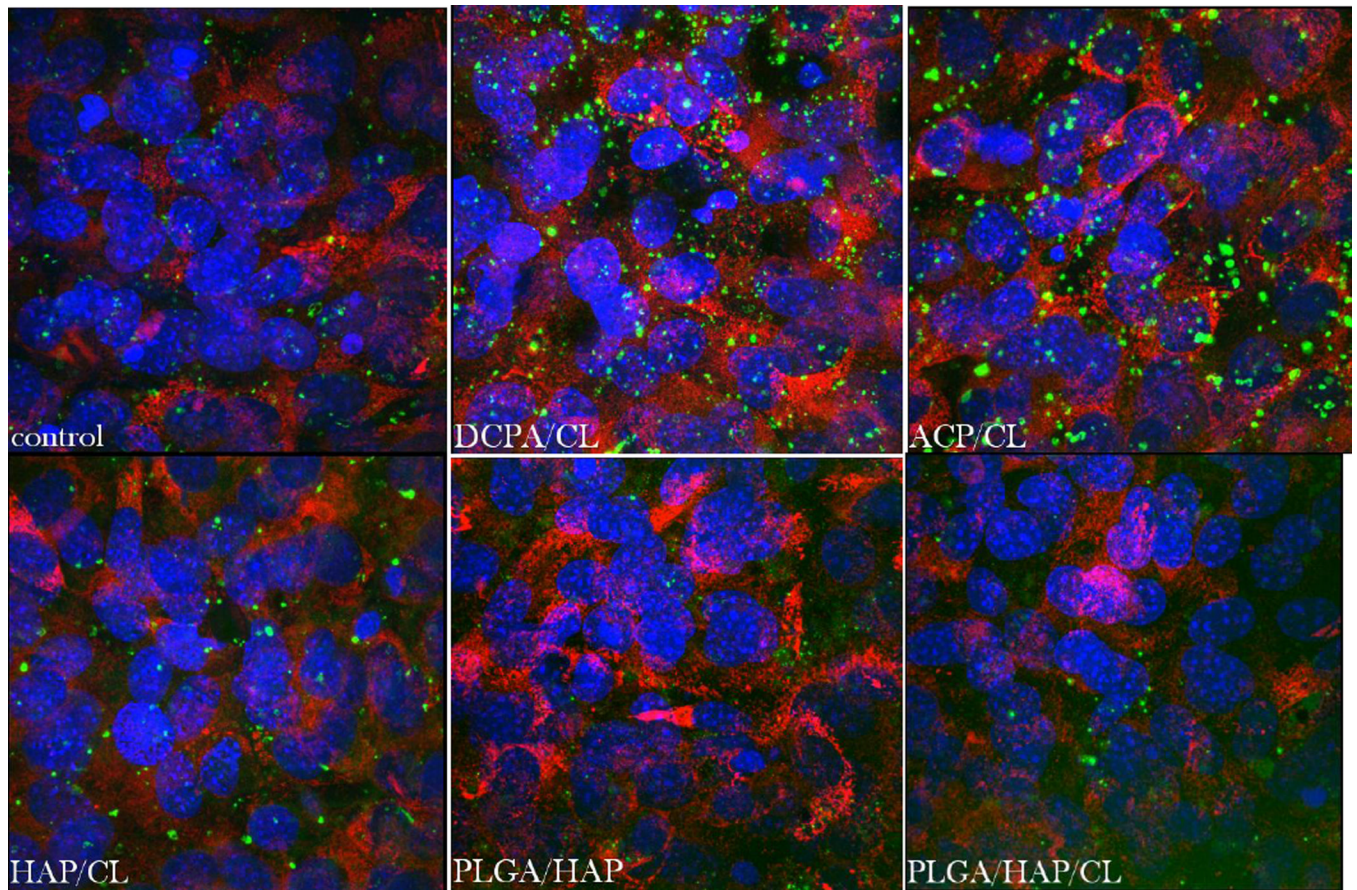
Fig.13.
Volume rendered confocal optical micrographs of fluorescently stained osteoblastic MC3T3-E1 cells (collagen type I - red; mineral particles – green; nucleus - blue) of the control sample and of those incubated with DCPA/CL, ACP/CL, HAP/CL, following 10 days of growth in differentiation media. The sizes of the images are 270 × 270 μm.
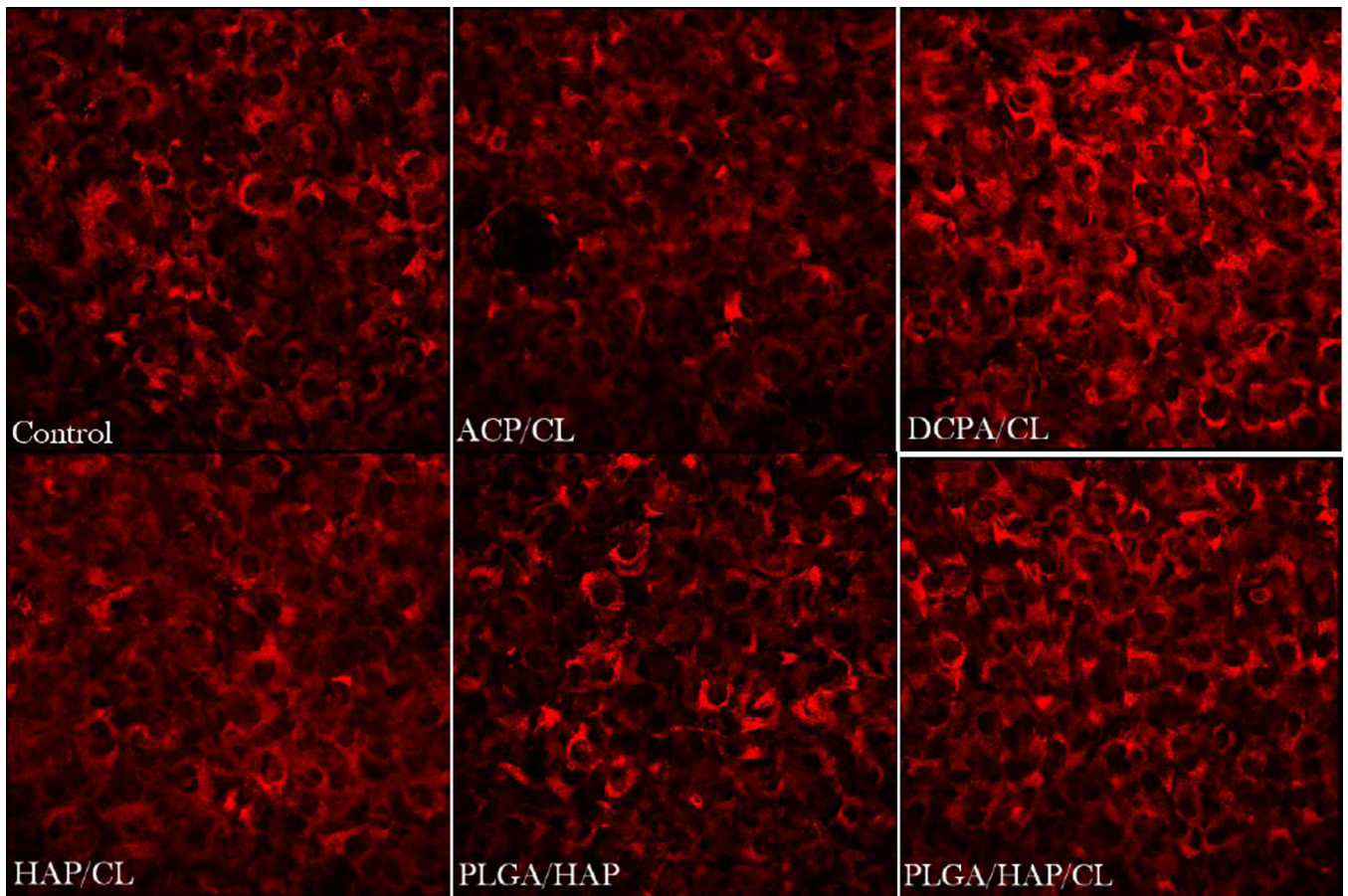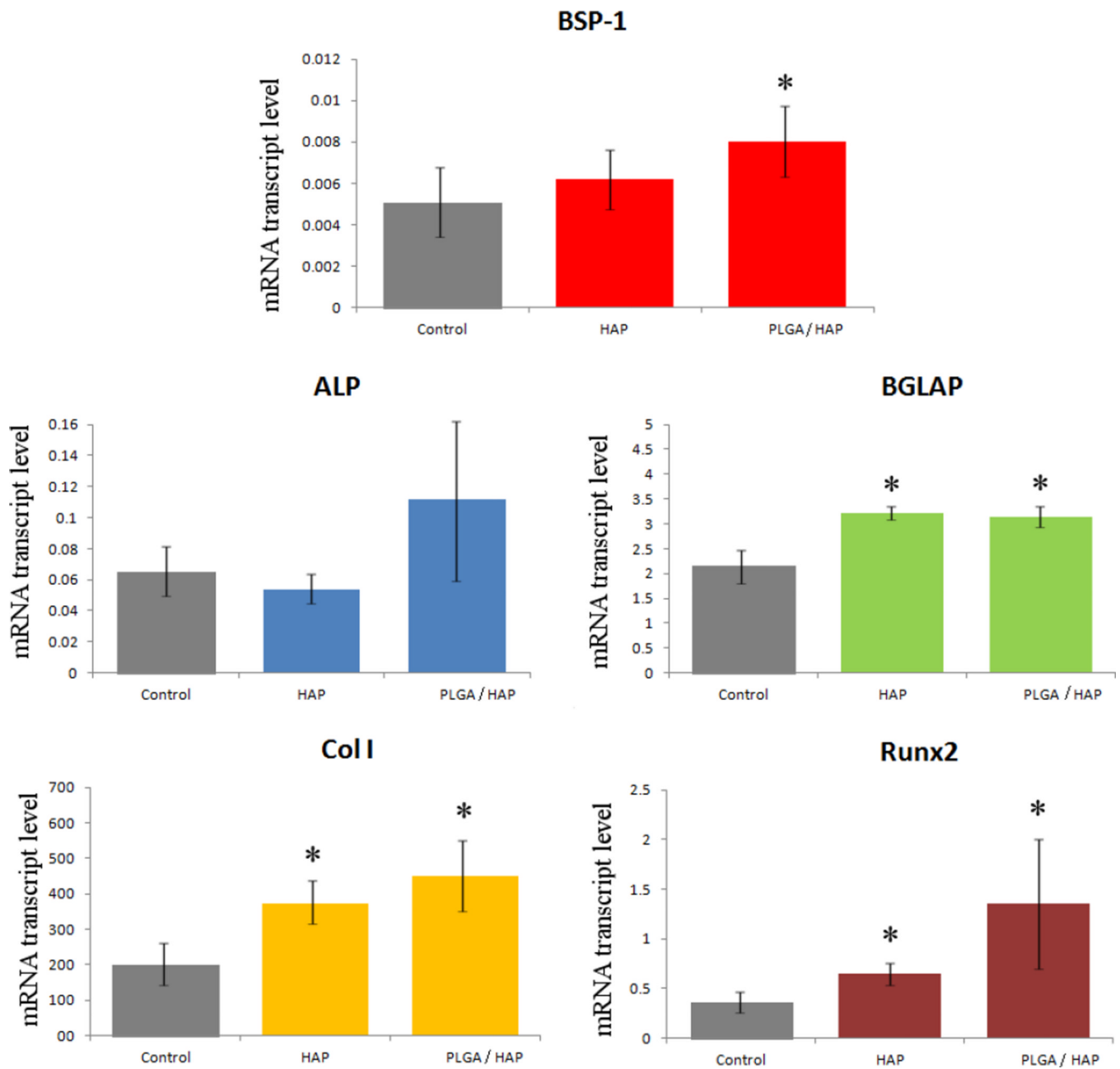
Fig.14.
Single-plane confocal optical micrographs of fluorescently stained collagen type I in osteoblastic MC3T3-E1 cells of the control sample (a) and of those incubated with PLGA/ HAP, PLGA/HAP/CL, DCPA/CL, ACP/CL and HAP/CL, following 10 days of growth in differentiation media. The sizes of the images are 675×675 μm.

Fig.15.
The comparative effect of HAP and PLGA/HAP particles loaded with CL on the mRNA expression of five different osteogenic markers: *BSP-1, ALP, BGLAP, Col I* and *Runx2* in osteoblastic MC3T3-E1 cells. mRNA expression was detected by quantitative RT-polymerase chain reaction relative to the housekeeping gene *ACTB*. Data normalized to expression of *ACTB* are shown as averages with error bars representing standard deviation. Genes significantly ($p < 0.05$) upregulated with respect to the control group are marked with *. No genes were significantly ($p < 0.05$) downregulated with respect to the control group.
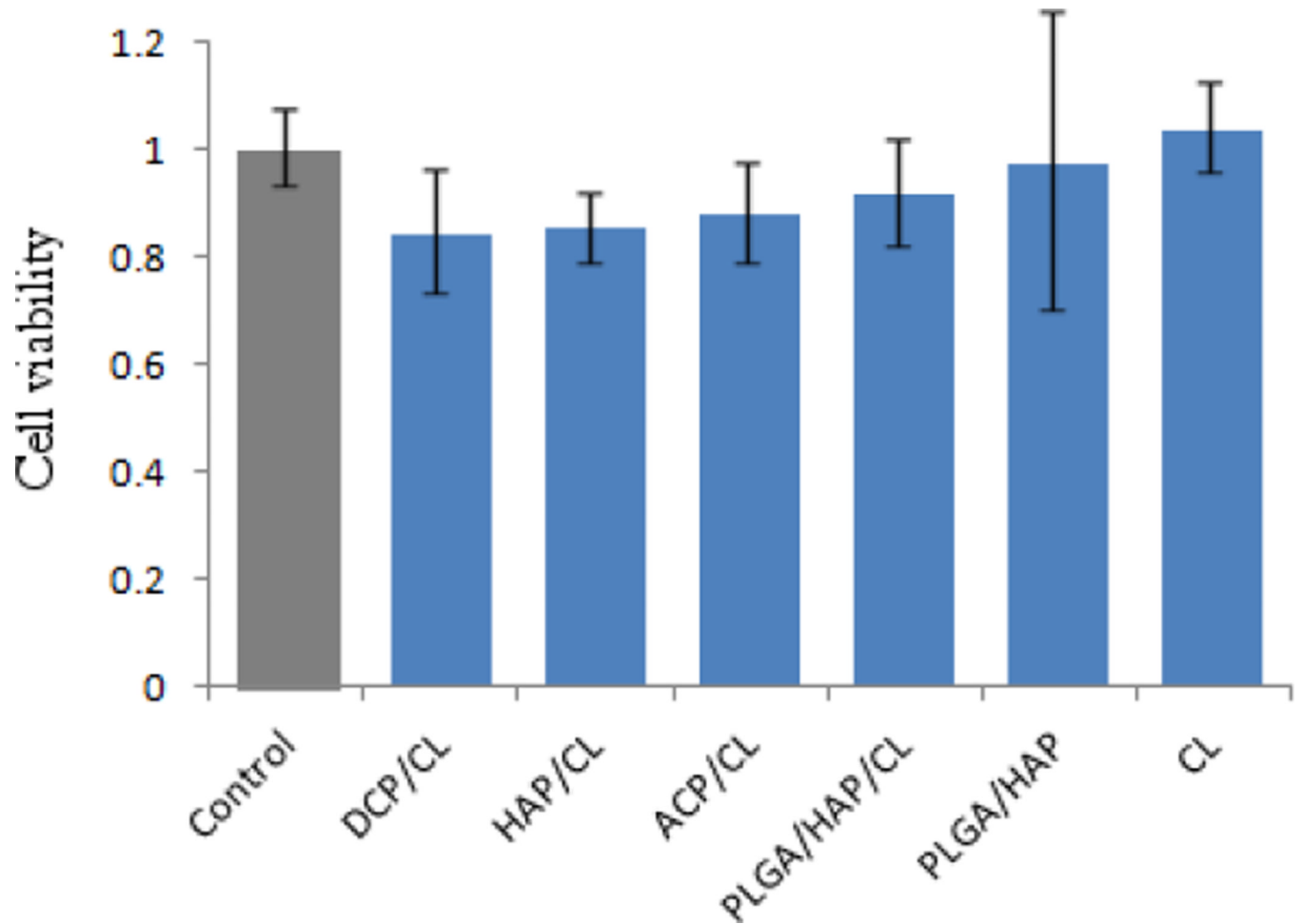
Fig.16.
Cell viability normalized to the negative control and determined by the MTT assay for different types of CLcontaining particles, including CL alone. Data normalized to the viability of the control sample are shown as averages with error bars representing standard deviation.

Table 1

CAP phases synthesized and analyzed for cell response.

Phase	Chemical formula	pK$_{sp}$ at 37 °C	Dissolution time[**]	Ca/P molar ratio
MCPM[*]	Ca(H$_2$PO$_4$)$_2$·H$_2$O	1.14	≈ 1–2 h	0.5
DCPA[*]	CaHPO$_4$	7.0	≈ 1 week	1
ACP[*]	Ca$_3$(PO$_4$)$_2$·nH$_2$O	25	≈ 3 months	1.3–1.5
HAP[*]	Ca$_{10}$(PO$_4$)$_6$(OH)$_2$	117.3	≈ 1 year	1.67

[*] MCPM = monocalcium phosphate monohydrate; DCPA = dicalcium phosphate anhydrous, a.k.a. monetite; ACP = amorphous calcium phosphate (data pertain to the phase obtainable at pH 9 – 11); HAP = hydroxyapatite.

[**] Measured in 1 mg/mL aqueous solution buffered with Tris/HCl (pH 7.40) and at 25 °C, involving daily replacements of the medium.

Table 2

MIC values for pure CL and different HAP and PLGA/HAP powders loaded with different amounts of CL.

Powder	CL (wt%)	MIC (mg/mL)
HAP	3	2 – 4
PLGA/HAP	1	1 – 2
PLGA/HAP	5	< 1
CL	100	0.03